International Scholarly Research Network
ISRN Metallurgy
Volume 2012, Article ID 732471, 16 pages
doi:10.5402/2012/732471

Review Article

Overview of Intermetallic Sigma (σ) Phase Precipitation in Stainless Steels

Chih-Chun Hsieh and Weite Wu

Department of Materials Science and Engineering, National Chung Hsing University, 250 Kuo-Kuang Road, Taichung 402, Taiwan

Correspondence should be addressed to Weite Wu, wwu@dragon.nchu.edu.tw

Received 14 December 2011; Accepted 19 January 2012

Academic Editors: M. Gjoka and Y. Yamabe-Mitarai

The σ phase which exists in various series of stainless steels is a significant subject in steels science and engineering. The precipitation of the σ phase is also a widely discussed aspect of the science and technology of stainless steels. The microstructural variation, precipitation mechanism, prediction method, and effects of properties of σ phase are also of importance in academic discussions. In the first section, a brief introduction to the development and the precipitation characteristics (including morphologies and precipitation sites) of σ phase in stainless steels is presented. In the second section, the properties effect, prediction method, processing effect, elemental addition, retardation method and Thermo-Calc simulation of the σ phase in stainless steels are highlighted.

1. Motivation

The precipitation of the σ phase, which is often observed in various series of stainless steels, is one of the main reasons for the deterioration of stainless steels' properties, for example, mechanical property, corrosion resistance, and weldability. The σ phase can be precipitated under an elevated temperature environment, for example, casting, rolling, welding, forging, and aging. It is difficult to prevent the precipitation of the σ phase when the Cr content is above a certain level (above 20 wt.%) in stainless steels. The addition of a strong ferrite stabilizer into the stainless steels (Cr, Si, or Mo) rapidly leads to the formation of the σ phase. This means that the transformation from δ-ferrite to the σ phase can be accelerated when the Cr, Si, or Mo diffuse efficiently in δ-ferrite. Hence, understanding the mechanism of the $\delta \rightarrow \sigma$ phase transformation is crucial to the prediction and control of stainless steels' properties. This review paper presents a comprehensive overview of the precipitation of the σ phase in stainless steels, and it is hoped that it will result in some scientific contributions in the materials science and engineering of stainless steels.

2. Review of Sigma Phase (σ)

2.1. Development Progress of the σ Phase.

(1) In 1907, Treitschke and Tammann found that the σ phase in the Fe-Cr binary system was an intermetallic compound of 30 wt.% Cr~50 wt.% Cr [1].

(2) In 1927, Bain and Griffiths observed the successful σ phase in the Fe-Cr-Ni ternary system. They found that the σ phase was a very hard and brittle compound which impacted the toughness of the steels. At that time, the σ phase was called the "B constituent" [2].

(3) In 1936, this Fe-Cr compound was called the "σ phase" by Jett and Foote, which became its official name [3].

(4) In 1951, the crystal structure of the σ phase in the Fe-Cr binary system was examined by Yano and Abiko They pointed out that the σ phase exhibited slower precipitation kinetics in the Fe-Cr alloy system than in the Fe-Cr-Mo and Fe-Cr-Si ternary systems [4].

Table 1: Chemical composition and lattice constant of the σ phase [10].

Alloy	Lattice parameter (Å)	Composition of phase (wt%)					Formula
		Fe	Cr	Ni	Mo	Si	
Fe-Cr	$a_0 = 8.799$, $c_0 = 4.544$						Fe-Cr
Fe-Mo	$a_0 = 9.188$, $c_0 = 4.812$						Fe-Mo
17Cr-11Ni-2Mo-0.4Ti	—		30	4.3	9	0.8	
17Cr-11Ni-0.9Mo-0.5Ti	—		33	4.5	5.4	0.7	
Type 316	$a_0 = 8.28\sim8.38$, $c_0 = 4.597\sim4.599$	55	29	5	11	—	$(FeNi)_x(CrMo)_y$
Type 316L	$a_0 = 9.21$, $c_0 = 4.78$						
20Cr-25-34Ni-6.5-8Mo	$a_0 = 8.87$, $c_0 = 4.61$	35/37	17/26	15/21	21/28	—	
25Cr-20Ni	—	40	46	9.4	—	3	

(5) In 1966, the σ phase was observed by Hattersley and Hume-Rothery [5] and Hall and Algie [6] in austenitic stainless steels.

(6) By 1966, the σ phase had been found in over 50 transition alloys [6], including Cr-Ni, Fe-Cr-Ni, Fe-Cr-Mo, Fe-Cr-Mn, Fe-Cr-Ni-Mo, Fe-Cr-Si, Fe-V, Re-Cr, Mo-Re, Ta-Al, W-Te, Ta-V, Zr-Ir, Nb-Pd, Ti-Mn, and Nb-Fe.

2.2. Precipitation Characteristic of the σ Phase. The σ phase is a tetragonal crystal structure, and its precipitation temperature is between 600°C and 1000°C [7–9]. The crystal information and chemical composition of the σ phase are listed in Table 1 [10]. The σ phase can increase the hardness and decrease the toughness, as well as the elongation, of steels [10]. The σ phase issues from the phase transformation of $\delta \rightarrow \sigma$ (δ-ferrite to σ phase). When the $\delta \rightarrow \sigma$ phase transformation occurs, the σ phase will precipitate in the high Cr-concentrated region of δ-ferrite and is formed directly in δ-ferrite particles. When the Cr content is below 20 wt.%, the precipitation of the σ phase is not readily observable in austenitic stainless steels [11]. However, the σ phase can be formed quickly when the Cr content is 25 wt.%~30 wt.%. Furthermore, the σ phase can also precipitate from γ-austenite when there is no δ-ferrite in the stainless steels [12]; albeit this is unlikely. The δ-ferrite is a Cr-rich region, compared to the γ-austenite, and it is a body-centered crystal (BCC) structure. Cr is easy to diffuse in δ-ferrite, and it is also a ferritic stabilizer. Hence, δ-ferrite is a beneficial site for the precipitation of the σ phase [13].

Shinohara et al. [14] pointed out that the precipitation of the σ phase was a diffusion-controlled phase transformation in 25% Cr-20% Ni stainless steel, and that the Cr atom had an important effect on the acceleration of the precipitation rate of the σ phase. The precipitation rate of the σ phase in δ-ferrite was higher (by about 100 times) than that of γ-austenite [15]. This meant that the diffusion velocity of the σ phase in δ-ferrite was faster than that in γ-austenite. The contents of Cr and Mo of δ-ferrite decreased and the Ni contents increased simultaneously after the σ phase precipitated. The above result led to the formation of secondary austenite phases (γ_2) via the δ-ferrite [16].

Figure 1 shows the Time-Temperature-Transformation (TTT) curve of the σ phase in various series of stainless steels [17]. It can be seen that the nose of the TTT curve is located at a temperature range of 800°C~850°C, which means that this temperature range has the fastest precipitation rate. Furthermore, the σ phase precipitates at 0.1 h in AISI 309S stainless steel, which has a higher precipitation rate than other stainless steels because of its high Cr content, low C content, and high δ-ferrite (15%).

Barcik [18] reported on the precipitation behavior of the σ phase in Cr-Ni austenitic stainless steel. His study found that the precipitated order of the σ phase was in triple point: δ-ferrite, incoherent twin boundary, and inclusion grain. Sikka pointed out that the σ phase was easy to precipitate at the δ/γ interphase boundaries [19] because the δ/γ interphase was a high boundary energy place and so a beneficial site for the heterogeneous nucleation of the σ phase. Sato et al. [20] found that a high lattice coherent degree and low δ/γ boundary energy could suppress the precipitation of the σ phase. Na et al. [21] found that the σ phase formed in γ-austenite when the aging time was high; they constructed a schematic diagram to explain the precipitation behavior of the σ phase, as shown in Figure 2. For Case 1, the σ phase was formed in γ-austenite, but needed a higher aging temperature (above 1000°C), as shown in Figure 2(a). For Case 2, the σ phase precipitated at the δ/γ interphase boundary because this boundary was a region of high boundary energy, as displayed in Figure 2(b). For Case 3, the σ phase precipitated in δ-ferrite particle and was attributed to the high Cr region of δ-ferrite. This precipitation behavior was the least difficult condition to accomplish, as represented in Figure 2(c). Padilha and Rios [22] pointed out that the σ phase precipitating directly in γ-austenite was very slow (about several thousand hours) [23]. Three main reasons for this were as follows.

(1) The σ phase was insoluble from C and N elements so that the precipitation time of the carbide and nitride was earlier than that of the σ phase.

(2) The σ phase was a second phase of a rich substitutional element. The diffusion of the substitutional element was very slow in γ-austenite so that the nucleation of the σ phase in γ-austenite was difficult.

(3) The crystallography of the σ phase and γ-austenite was incoherent.

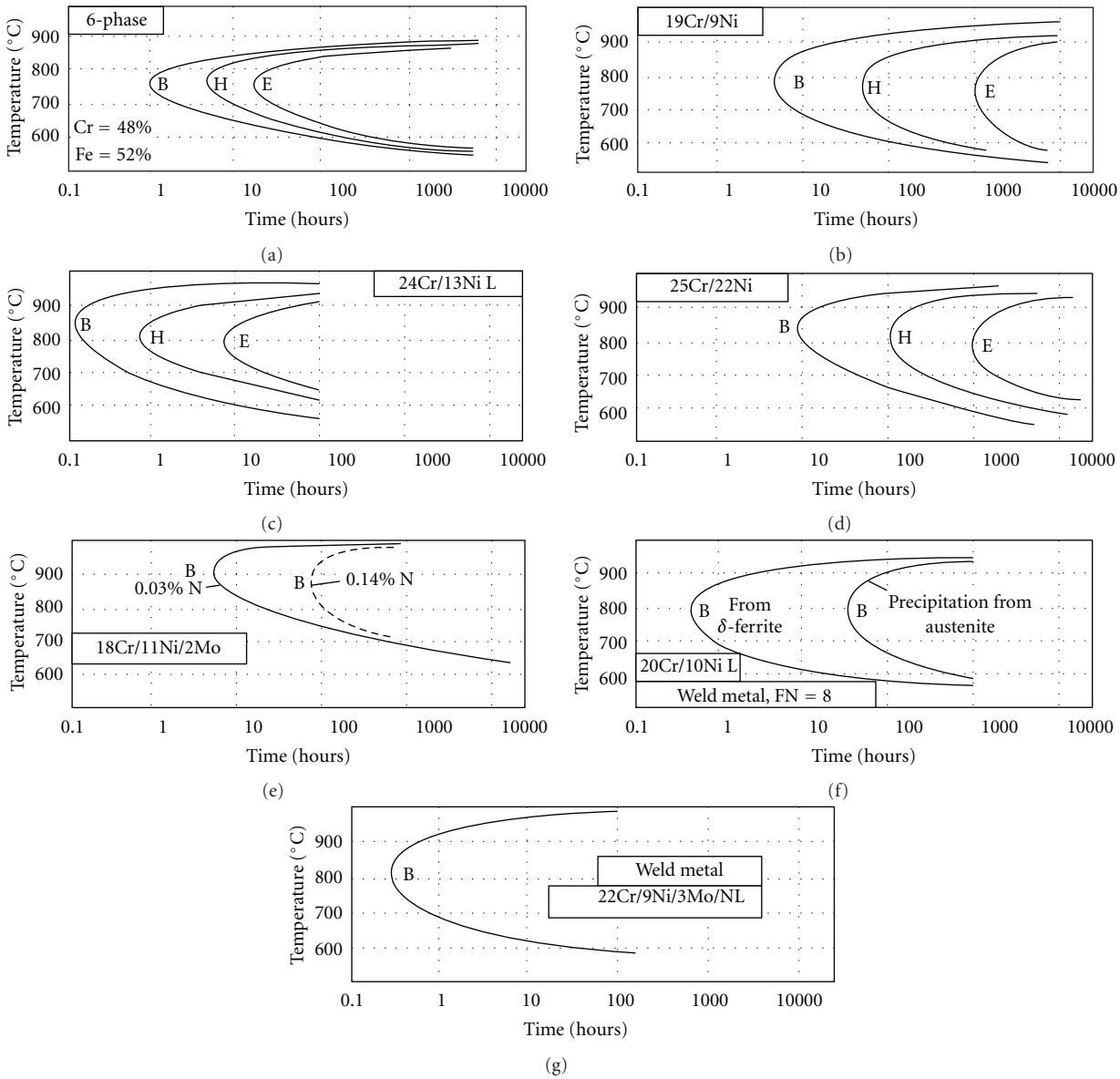

Figure 1: TTT curves of the σ phase in various series of stainless steels (B: initial precipitation, H: intermediate stage, E: final precipitation stage [17].

2.3. Microstructural Characteristic of the σ Phase. In 1978, Gray et al. [24] used an advanced magnetic etching technique to observe the $\delta \rightarrow \sigma + \gamma_2$ phase transformation. Figures 3 and 4 show the microstructures of AISI 304 stainless steel aged at 595°C and 650°C for 31000 h, respectively, using magnetic etching. The plate σ phase and γ_2 precipitate in δ-ferrite particles. Therefore, the precipitation of the σ phase is via the eutectoid decomposition of $\delta \rightarrow \sigma + \gamma_2$. The σ phase has a similar precipitation mechanism when aged at 650°C for 31000 h, but the eutectoid decomposition of $\delta \rightarrow \sigma + \gamma_2$ is more evident in this condition.

This Section introduces the morphologies of the σ phase in austenitic, ferritic, and duplex stainless steels.

2.3.1. Austenitic Stainless Steels. Figure 5(a) shows the as-casting microstructure of the σ phase in AISI 309 LSi stainless steel, and then the σ phase precipitating in dendrite δ-ferrite [25]. This is the typical precipitation morphology of the σ phase. Figure 5(b) shows the microstructure of the σ phase in as-rolled AISI 316 stainless steel [26]. The σ phase is indicated by a lacy structure and precipitates with a fixed crystallographic direction because of the rolling function. Figure 5(c) shows the as-rolled microstructure of the σ phase with a 50% rolling ratio in AISI 304 stainless steel, and the σ phase exhibits dispersed globular morphologies [27]. This globular structure is a stable morphology.

2.3.2. Ferritic Stainless Steels. Generally, many secondary phases (e.g., χ phase, Lave phase, etc.) exist in ferritic stainless steels, so that a microstructural examination of the σ phase is necessary. The microstructures of the σ phase were studied in

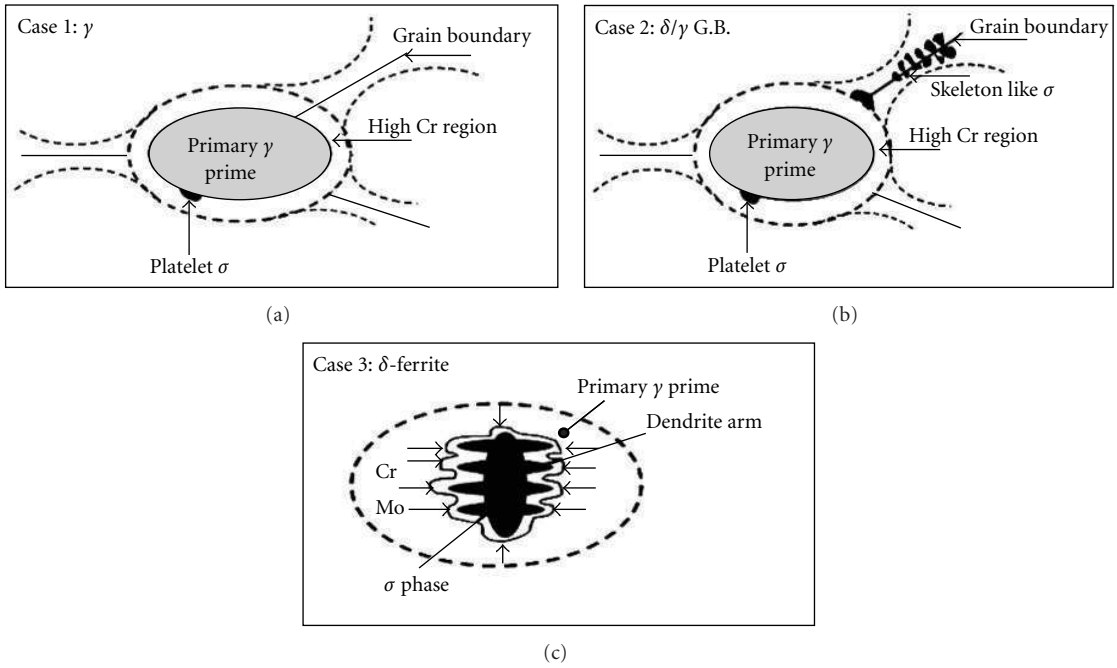

Figure 2: Schematic diagram of the σ phase precipitation [21].

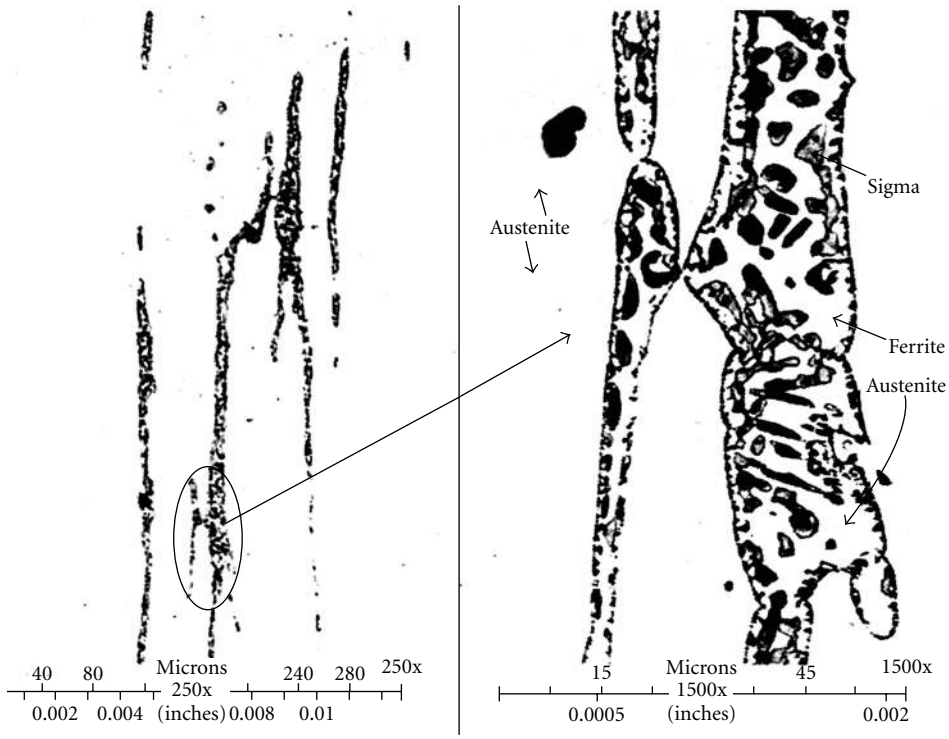

Figure 3: Microstructural observation of the $\delta \rightarrow \sigma + \gamma_2$ phase transformation in AISI 304 stainless steel (595°C, 31000 hr) [24].

Fe-29Cr-8W ferritic stainless steel aged at 850°C for different aging times [28]. The σ phase can precipitate obviously above 10 h. However, the precipitation mechanism of the σ phase accompanies the χ phase in the δ-ferrite matrixes as compared to austenitic stainless steels.

2.3.3. Duplex Stainless Steels. The microstructure of the σ phase was studied after heat treatment in A905 duplex stainless steel [26]. The σ phase (bright phase) precipitates in δ-ferrite grains when the aging condition is 30 min at 1100°C + 1 h at 900°C. However, $\sigma + \gamma_2$ cellular structures form in

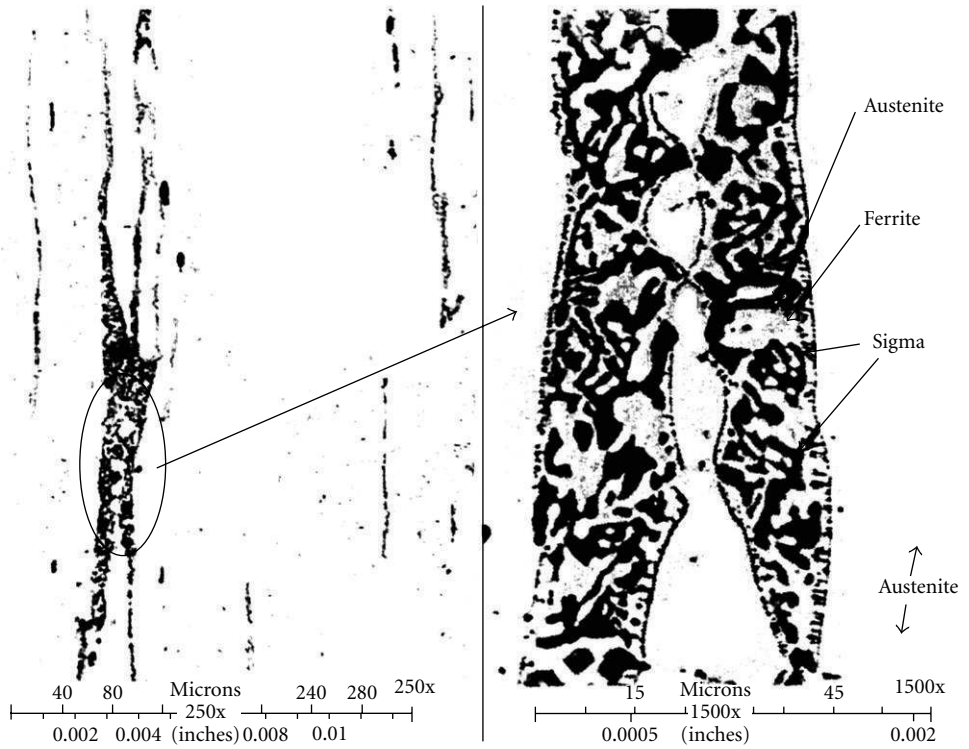

Figure 4: Microstructural observation of the $\delta \rightarrow \sigma + \gamma_2$ phase transformation in AISI 304 stainless steel (650°C, 31000 hr) [24].

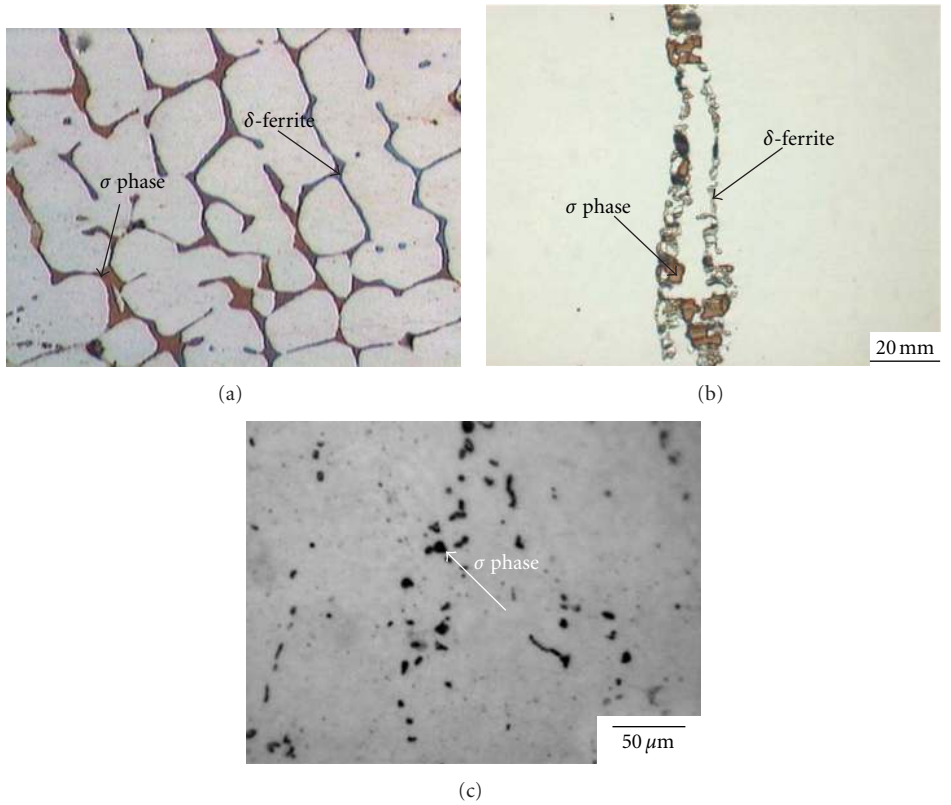

Figure 5: Microstructural observation of the σ phase with different working conditions in the austenitic stainless steels (a) as casting AISI 309 LSi stainless steel, (b) as rolled AISI 316 stainless steel, (c) with 50% rolling ratio in AISI stainless steel [25].

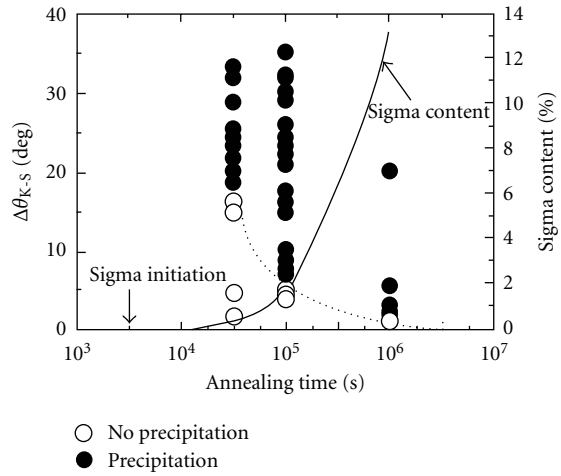

FIGURE 6: Effect of the deviation angle $\Delta\theta_{K\text{-}S}$ and the annealing time on the formation of σ phase at δ/γ interfaces in the weld metal [20].

δ-ferrite particles when the aging situation is 30 min at 1100°C + 10 h at 900°C. Finally, δ-ferrite is consumed by the $\sigma + \gamma_2$ cellular structures completely when the aging condition is 30 min at 1100°C + 10 h at 800°C.

2.4. Classification of Morphologies of the σ Phase. In stainless steels, classification of the morphology of the σ phase can be divided into four types: (1) grain boundary precipitation, (2) triple point precipitation, (3) corner precipitation, and (4) cellular precipitation [29]. A discussion of these four morphologies follows.

2.4.1. δ/γ Grain Boundary Precipitation. The σ phase is easy to precipitate at the δ/γ phase boundary, which is a high Cr region. When a high Cr region forms, the depleted Cr region is also formed and leads to a decrease in the corrosion resistance at the same time. Furthermore, the δ/γ interphase boundary is a high interface energy site, and, as many defects concentrate there, it is a beneficial site for the heterogeneous nucleation of the σ phase. When the σ phase nucleates at the δ/γ interphase boundary, some defects disappear, which releases the free energy of the materials. Consequently, this decreases the activation energy barrier to form a coherent interface. Sato and Kokawa [30] pointed out that the σ phase forms preferentially at one side of the δ/γ interfaces along intergranular austenite in duplex stainless steel weld metal annealed at 1100 K. The crystallographic orientation relationships at the δ/γ interfaces are the σ phase forms which have deviated largely from the K-S relationship ($\Delta\theta_{K\text{-}S}$), as shown in Figure 6. The minimum deviation angle for the sigma phase formation decreases with increasing annealing time. Furthermore, the formation of the σ phase is strongly affected by the coherency and interfacial energy of the δ/γ interface.

2.4.2. Triple Point Precipitation. The σ phase precipitates at the triple point of the δ-ferrite boundary and this precipitation type, called the "triple point σ phase." Barick [31] pointed out that the formation of the triple point σ phase must be aged below 600°C for 10000 h~15000 h. The triple point σ phase also forms at the incoherent twin boundaries and the intragranular inclusions.

2.4.3. Corner Precipitation. The corner precipitation of the σ phase means that the σ phase forms directly in corner δ-ferrite particles because the δ-ferrite is a high Cr content phase, and σ phase prefers to nucleate and precipitate at that point. When the σ phase precipitates at the corner δ-ferrite, it consumes the Cr content of the δ-ferrite particles.

2.4.4. Cellular Precipitation. Cellular precipitation means that the σ phase and secondary austenite ($\sigma + \gamma_2$) precipitate as laminar precipitation in the δ-ferrite particles. This reaction is called the eutectoid decomposition of $\delta \rightarrow \sigma + \gamma_2$. When the eutectoid decomposition of $\delta \rightarrow \sigma + \gamma_2$ is finished, the σ phase consumes the Cr, Mo, and Si contents of the δ-ferrite particles.

2.5. Precipitation of the σ Phase in Austenitic, Superferritic, and Duplex Stainless Steels. Villanueva et al. [32] discussed the precipitation mechanism of the σ phase in the as-rolled plate of AISI 316L austenitic (17Cr-12Ni-2.4Mo), DIN 1.4574 superferritic (28Cr-4Ni-2.4Mo-0.31Nb), and UNS S31803 duplex (22Cr-5.4Ni-2.4Mo) stainless steels with various aging temperatures. Three schematic diagrams (Figures 7–9) can be used to explain the precipitation mechanism of σ phase.

Figures 7(a)–7(d) show the precipitation mechanism of σ phase in AISI 316L stainless steel at different aging temperatures. Without heating (T_0), the δ-ferrite is indicated by a lacy structure and precipitates at the δ/γ interphase boundary and γ phase. When the aging temperature is increased to T_1, the σ and γ_2 phases precipitate in δ-ferrite particles. When the aging temperatures are increased to T_2, the cellular $\sigma + \gamma_2$ also forms in δ-ferrite particles, and the σ phase precipitates at the triple points and the δ/γ interphase boundaries. When the aging temperature is T_3, the precipitation of the laminar $\sigma + \gamma_2$ is more obvious than at the other aging temperatures.

Figures 8(a)–8(d) show the precipitation of σ phase in superferritic stainless steel. There is only δ-ferrite and no precipitation of the σ phase without heating (T_0) in superferritic stainless steel. When the aging temperature is T_1, the σ phase can occupy the triple points of the δ-ferrite grain boundaries. The σ phase grows at the δ-ferrite grain boundaries completely when the aging temperature increases to T_2. Finally, the σ phase precipitates and extends to the inner δ-ferrite grain when the aging temperature is raised to T_3.

Figures 9(a)–9(d) are the precipitation mechanism of σ phase in UNS S31803 duplex stainless steel. Here are δ and γ phases in UNS S31803 duplex stainless steel without heating (T_0). Some laminar cellular structures ($\sigma + \gamma_{New}$) are formed at the δ/γ interphase boundaries when the aging temperature is T_1. Furthermore, the laminar cellular structures continue to grow when the aging temperature is increased to T_2. Finally, the δ-ferrite is occupied completely.

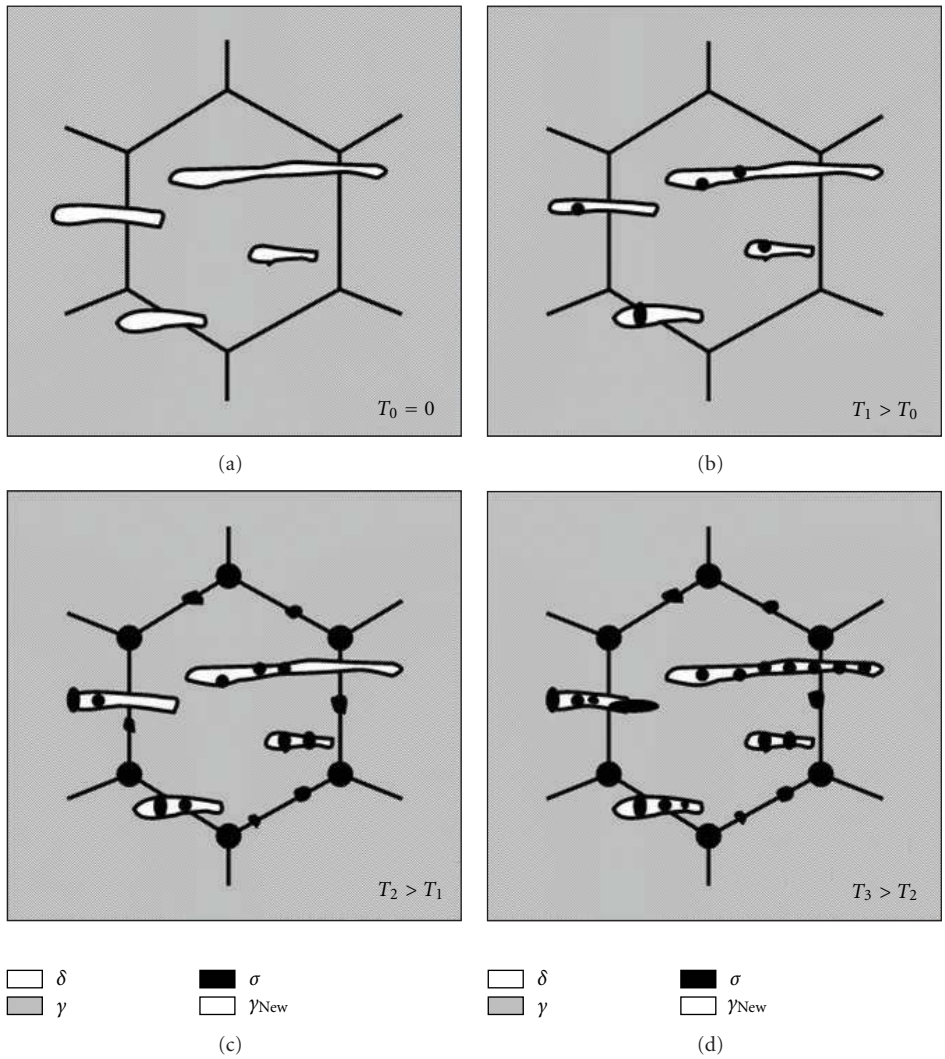

Figure 7: Precipitation mechanism of the σ phase in AISI 316L stainless steel [32].

Villanueva et al. [32], in describing the above results, pointed out the precipitation level of the σ phase: Duplex stainless steel > Superferritic stainless steel > Austenitic stainless steel.

2.6. Effect of the σ Phase on the Properties of Stainless Steels

2.6.1. Formation of Brittle Region. The embrittlement region of the σ phase forms in a temperature range of 650°C~ 900°C during the welding process in austenitic stainless steels. Hence, the welding energy and cooling rate must be controlled during welding in order to prevent the grain growth and precipitation of the brittle σ phase because the precipitation of the σ phase decreases the toughness and elongation. An embrittlement region of σ phase can be shown in Shaeffler diagram of Figure 10 [33]. Figure 10 of gray region is embrittlement region of σ phase, and this region is the widest in the mixed austenite plus ferrite phase region (A + F). On the other hand, the single austenite phase region (A) shows a small embrittlement range of the σ phase. Therefore, the possibility of the σ phase is lower in austenitic stainless steels. However, increasing the Cr content can promote the precipitation of the σ phase.

2.6.2. Extension of Hot Cracking during Welding. Konosu et al. [34] observed hot cracking in three stainless steel weld metals and the hot cracking extends along the γ/σ interface boundaries. The γ/σ interface boundaries are an initial fracture position of low elongation. This crack is a beneficial site and acts as a nucleated point of the σ phase. The growth of hot cracking cannot be neglected as it is very significant during the welding. Mataya and Carr [35] pointed out that hot cracking occurs because of the $\delta \rightarrow \sigma$ phase transformation in the 21Cr-6Ni-9Mn austenitic stainless steel.

2.6.3. Formation of Depleted Cr Region and Reduction of Corrosion Resistance. The precipitation of the σ phase reduces the corrosion resistances to the intergranular, pitting, and crevice. Reis et al. [36] reported that pitting corrosion

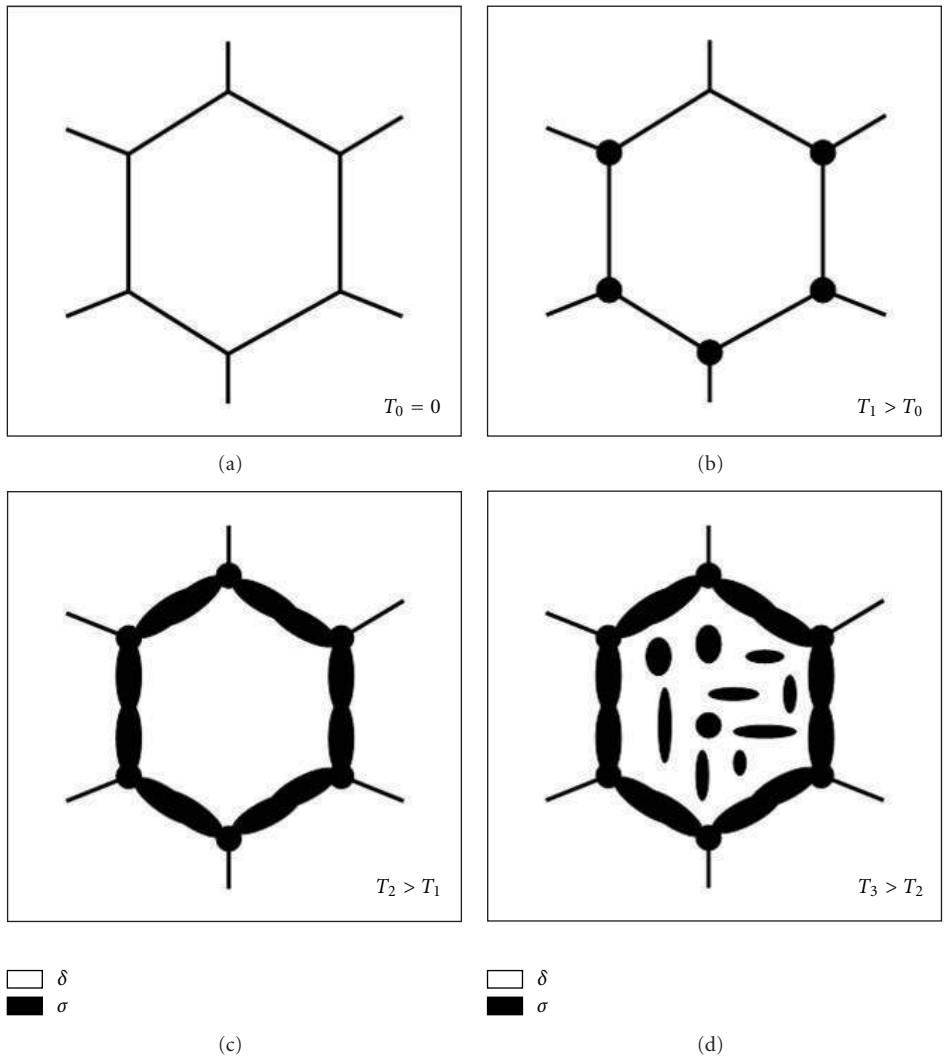

Figure 8: Precipitation mechanism of the σ phase in DIN 1.4575 stainless steel [32].

resistance has an important relationship with the Cr content. Hence, pitting corrosion always happens at low Cr content points. Generally, the austenitic boundary is a preferential site for pitting corrosion because the austenite has a low Cr content. However, the depleted Cr zone disappears gradually as a function of Cr diffusion, which issues from the austenite but not the δ-ferrite. The σ phase always forms at the δ/γ interface boundaries and causes the formation of a depleted zone [37]. The σ phase and γ-austenite induce the galvanic effect, and the γ-austenite is corroded preferentially. Consequently, the corrosion potent is decreased. The fine σ phase has a more obvious effect on intergranular corrosion resistance than does the coarser σ phase because the fine σ phase forms a networked structure at the interface, and the coarse σ phase precipitates independently at the interface. Ravindranath and Malhotra [38] pointed out that intergranular corrosion resistance has an important effect on the formation of the networked σ phase. Besides, an independent coarse σ phase has no influence on intergranular corrosion resistance.

2.7. Prediction Methods of the σ Phase. Chemical composition can be used to predict the precipitation of the σ phase. Gow and Harder [39] pointed out an empirical formula to examine the precipitation tendency of the σ phase, as expressed in(1)

$$\text{Ratio factor} = \frac{\%\text{Cr} - 16\%\text{C}}{\%\text{Ni}}. \tag{1}$$

If ratio factor >1.7, the σ phase can precipitate in stainless steels. When the C content is much higher, the ratio factor is much lower, and the precipitation tendency of the σ phase is decreased.

Woodyatt [40] also pointed out a predicted formula of the σ phase via an electron vacancy number (at. %), as represented in(2)

$$N_v = 0.66\text{Ni} + 1.71\text{Co} + 2.66\text{Fe} + 4.66(\text{Cr} + \text{Mo} + \text{W}) + 5.66\text{V} + 6.66\text{Zr} + 10.66\text{Cb}. \tag{2}$$

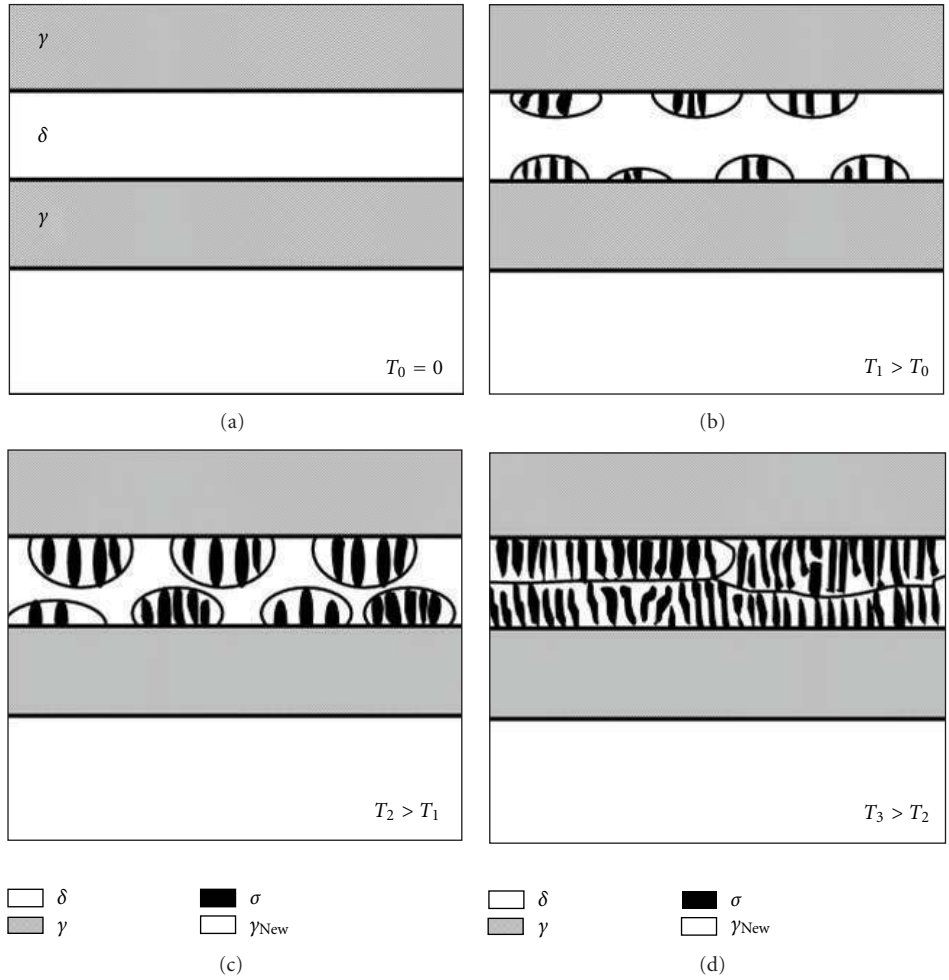

Figure 9: Precipitation mechanism of the σ phase in UNS S31803 stainless steel [32].

When the electron vacancy number ($\overline{N_v}$) > 2.52, the σ phase can be formed in stainless steels. According to Woodyatt's theory, the $\overline{N_v}$ in the AISI 310 stainless steel is equal to 2.88, so that this stainless steel indicates the precipitation of the σ phase. However, the interstitial elements (C and N) are neglected in this prediction formula.

Hull [41] pointed out an empirical formula to predict the σ phase precipitation, as exhibited in (3). This equation has been widely used because it takes into account many alloy elements.

$$\mathrm{Cr_{eq}} = \mathrm{Cr} + 0.31\mathrm{Mn} + 1.76\mathrm{Mo} + 0.97\mathrm{W} + 2.02\mathrm{V} + 1.58\mathrm{Si} + 2.44\mathrm{Ti} + 1.70\mathrm{Cb} + 1.22\mathrm{Ta} - 0.266\mathrm{Ni} - 0.177\mathrm{Co}. \quad (3)$$

2.8. Retardation Methods of the σ Phase

2.8.1. Solid Solution Heat Treatment. The precipitation of the σ phase can be retarded by the use of the solid solution heat treatment. When stainless steels are heated to above 1050°C, the σ phase diffuses and dissolves into the γ-austenite matrix [42]. This dissolution process is called the "$\sigma \rightarrow \gamma$ phase transformation."

2.8.2. Subsequent Rolling Process. Gill et al. [43] reported that the dendrite σ phase is an unstable morphology and can lead to embrittlement of the stainless steels. The subsequent rolling process can be used to refine the σ phase particles from an unstable dendrite into stable globular morphologies. Hence, the embrittlement of the σ phase is decreased in the stainless steels by the subsequent rolling process.

2.8.3. Addition of Alloy Elements. In recent years, Ni has been used to replace N and decrease the N addition because the price of the Ni in steel continues to improve. Lin et al. [44] reported that N addition decreases the δ-ferrite content during the nitrogen atmospheric aging heat treatment and retards the phase transformation from δ to σ. However, C has a similar effect on the suppression of the σ phase, but its addition leads to the precipitation of the nitride and causes sensitization and embrittlement.

Brandis et al. [45] pointed out that Nitrogen had a better effect on the retardation of the σ phase than Carbon. Smuk et al. [46] studied the powder metallurgy of duplex stainless steels and found that Cu particles could pin the σ/γ_2 interface boundaries, as shown in Figure 11. This meant that the

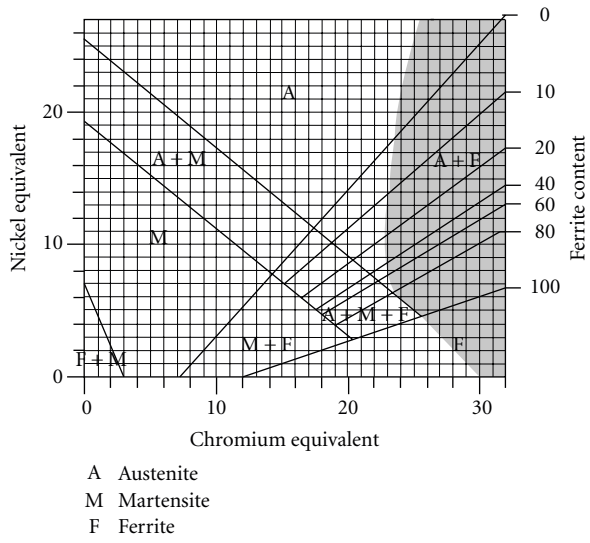

Figure 10: Shaeffler diagram showing the embrittlement region of the σ phase [33].

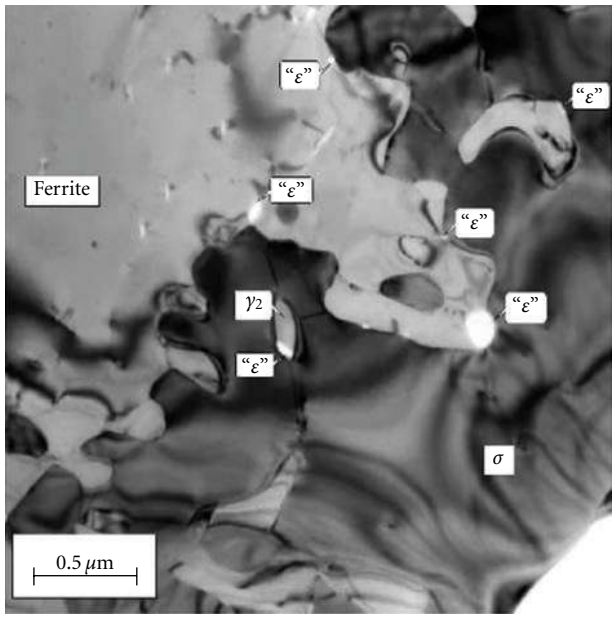

Figure 11: Cu particles can pin and prevent the motion of the σ/γ_2 interface [46].

Cu particles could prevent the motion of the σ/γ_2 interface boundaries and can change the morphologies of the σ phase. Consequently, the $\delta \rightarrow \sigma$ phase transformation could be suppressed efficiently.

2.9. Thermo-Calc Simulation of the σ Phase. Besides the metallographic technique and quantitative analysis, the precipitation examination of the σ phase can also be predicted using a Thermo-Calc software simulation. This thermodynamic simulation only needs the input of the element contents and experimental temperatures to produce the phase diagrams. This simulation method is called Calculation of Phase Diagrams (CALPHAD).

The simulation methods of the Thermo-Calc software in the σ phase have three databases: Steel & Fe-Alloys Database (TCFE), SGTE Solution Database (SSOL) [47] + Lindholm [48], and Modified SSOL [49]. Erneman et al. [49] used the three Thermo-Calc databases (TCFE, SSOL + Lindholm, Modified SSOL) to calculate the σ phase fraction in AISI 347 stainless steel at 700°C. The σ phase has a lesser volume fraction, which means a lower grain growth according to the TCFE simulation result. The simulation result of the Modified SSOL indicates a higher volume fraction of the σ phase, which means a higher grain growth. The simulation data of SSOL was in between the TCFE and SSOL databases. Saunders and Miodownik [50] used the Thermo-Calc software to simulate the precipitation quality of the σ phase with Mo, Mn, So, N, and C in Fe-22Cr-5.5Ni stainless steel between 670°C and 850°C. The series of simulation results were shown in Figures 12(a)–12(f). However, by adding 3% Mo into the original stainless steel, this steel becomes Fe-22Cr-5.5Ni-3Mo stainless steel, as shown in Figure 12(b). This CAPLAD result indicates that the σ phase has the highest content of all temperatures at 800°C. Moreover, Mo addition can extend the precipitation range to 900°C.

By adding 1.7% Mn into the Fe-22Cr-5.5Ni-3Mo stainless steel, this steel becomes Fe-22Cr-5.5Ni-3Mo-1.7Mn stainless steel. The CALPHAD result shows that Mn has a competitive effect with Cr and Mo, so it can promote the precipitation of the σ phase, as shown in Figure 12(c). By adding 0.4% Si into the Fe-22Cr-5.5Ni-3Mo-1.7Mn, this steel becomes Fe-22Cr-5.5Ni-3Mo-1.7Mn-0.4Si stainless steel. The CALPHAD result shows that Si is a strong ferrite stabilizer which can raise the σ phase content, as indicated in Figure 12(d). Hence, it can be concluded that Si promotes the $\delta \rightarrow \sigma$ phase transformation. By continuing to add 0.14N into the Fe-22Cr-5.5Ni-3Mo-1.7Mn-0.4Si, this steel becomes Fe-22Cr-5.5Ni-3Mo-1.7Mn-0.4Si-0.14N stainless steel. When N is added, the nitride (M_2N) forms, and the σ phase content decreases at the same time, as shown in Figure 12(e). This is because N addition promotes the $\delta \rightarrow \gamma$ phase transformation and retards the $\delta \rightarrow \sigma$ phase transformation.

Similarly, by adding 0.24C to the Fe-22Cr-5.5Ni-3Mo-1.7Mn-0.4Si-0.14N, this steel becomes Fe-22Cr-5.5Ni-3Mo-1.7Mn-0.4Si-0.14N-0.24C stainless steel. The CALPHAD result shows that C addition leads to the formation of $M_{23}C_6$, as shown in Figure 12(f). The content of carbide is higher, and the content of σ phase is lower in stainless steels. Furthermore, the σ phase fraction with the C addition is lower than that with Mn, Si or N additions.

2.10. Effect of Various Processes on the σ Phase

2.10.1. Effect of Solid Solution-Treated Temperature and Cooling Rates on the σ Phase. Chen and Yang [51] studied 2205 duplex stainless steel as the solid solution treated at 1020°C with different cooling rates ($1°C\,s^{-1}$, $0.5°C\,s^{-1}$, $0.25°C\,s^{-1}$,

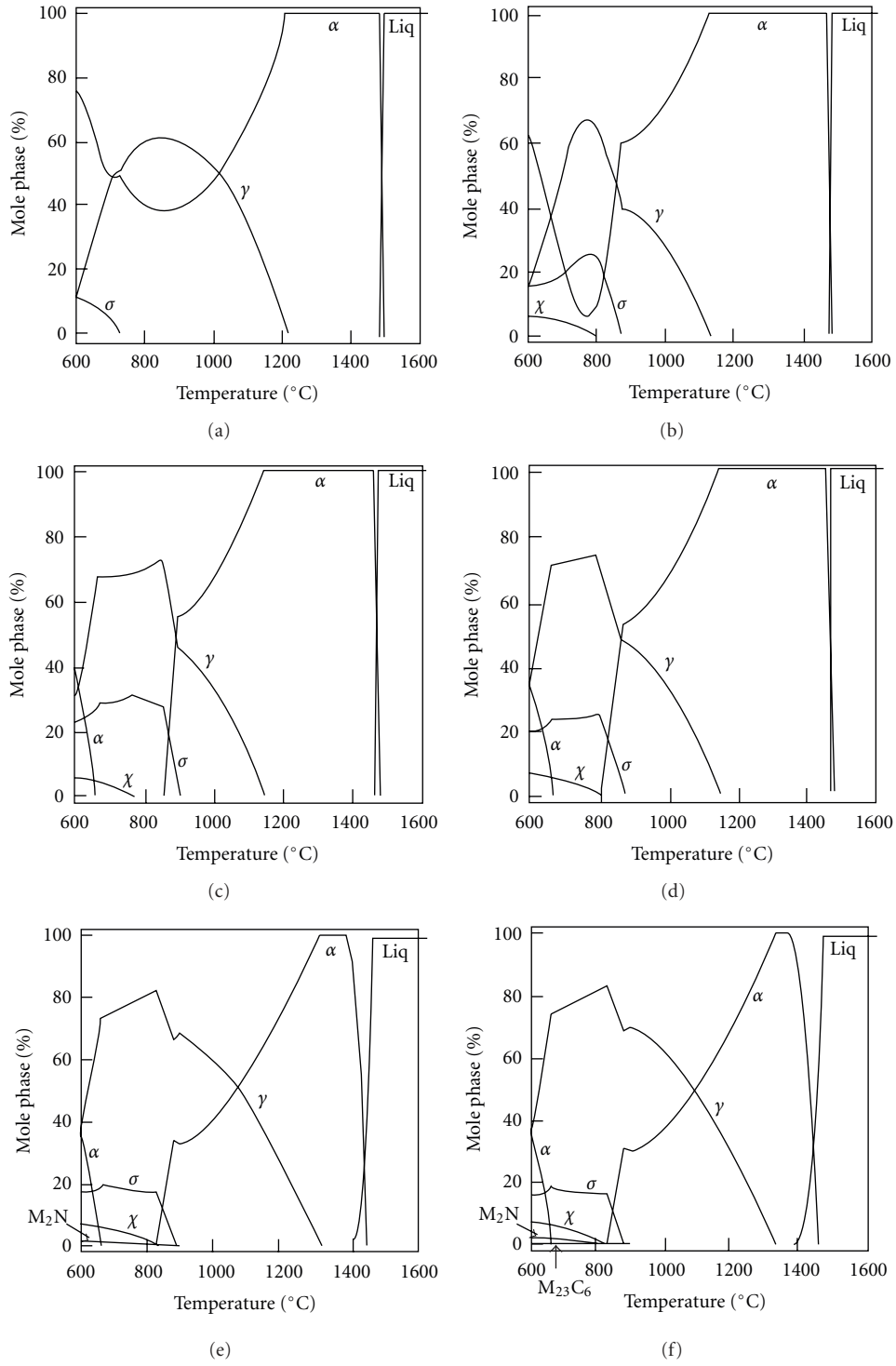

Figure 12: CALPHAD result of the phases (a) Original Fe-22Cr-5.5Ni, (b) Fe-22Cr-5.5Ni-3MoFe-22Cr-5.5Ni, (c) Fe-22Cr-5.5Ni-3Mo-1.7MnFe-22Cr-5.5Ni, (d) Fe-22Cr-5.5Ni-3Mo-1.7Mn-0.4Si, (e) Fe-22Cr-5.5Ni-3Mo-1.7Mn-0.4Si-0.14N, and (f) Fe-22Cr-5.5Ni-3Mo-1.7Mn-0.4Si-0.14N-0.24C stainless steels [46].

and $0.1^{\circ}\mathrm{C\,s^{-1}}$). The results showed that there was no σ phase when cooling rates were $1^{\circ}\mathrm{C\,s^{-1}}$ and $0.5^{\circ}\mathrm{C\,s^{-1}}$. The cooling rates of $0.25^{\circ}\mathrm{C\,s^{-1}}$ and $0.1^{\circ}\mathrm{C\,s^{-1}}$ indicated a slight σ phase and a lot of σ phases, respectively. On the other hand, the precipitation of the σ phase was concentrated mainly at the δ/γ interface boundaries and δ-ferrite. However, Chen and Yang [51] also observed the precipitation of the σ phase at two solid solution temperatures, 1020°C and 1080°C. Experimental result indicated that the content of the σ phase was higher with the cooling rate at 1020°C than at

Table 2: EDS analysis of δ, σ, and γ phases at various solid solution temperatures and a fixed cooling rate of $0.1^{\circ}C\,s^{-1}$ [51].

Element	Fe	Cr	Ni	Mo	Mn	Si
Solution treated at 1020°C and cooled at $0.1^{\circ}C\,s^{-1}$						
σ	61.7 ± 0.5	25.7 ± 0.6	3.46 ± 0.06	6.84 ± 0.08	1.15 ± 0.04	1.15 ± 0.04
δ	66.6 ± 0.7	24.1 ± 0.4	3.60 ± 0.06	4.09 ± 0.06	1.15 ± 0.04	0.44 ± 0.02
γ	68.0 ± 0.7	20.8 ± 0.4	6.45 ± 0.08	2.42 ± 0.06	1.45 ± 0.04	0.32 ± 0.02
Solution treated at 1080°C and cooled at $0.1^{\circ}C\,s^{-1}$						
σ	62.7 ± 0.5	25.2 ± 0.6	3.92 ± 0.06	5.90 ± 0.08	1.14 ± 0.04	1.13 ± 0.04
δ	66.7 ± 0.7	24.0 ± 0.4	3.68 ± 0.06	4.05 ± 0.06	1.15 ± 0.04	0.43 ± 0.02
γ	68.3 ± 0.7	20.9 ± 0.4	6.39 ± 0.08	2.45 ± 0.06	1.44 ± 0.04	0.33 ± 0.02
Solution treated at 1200°C and cooled at $0.1^{\circ}C\,s^{-1}$						
δ	67.0 ± 0.7	23.6 ± 0.4	3.83 ± 0.08	3.96 ± 0.06	1.16 ± 0.04	0.41 ± 0.02
γ	68.2 ± 0.7	21.3 ± 0.4	6.25 ± 0.08	2.54 ± 0.06	1.33 ± 0.04	0.35 ± 0.02

1080°C. Finally, Chen and Yang [51] used a solid solution temperature (1200°C) at a fixed cooling rate ($0.1^{\circ}C\,s^{-1}$) to discuss the precipitation of the σ phase. The experimental result showed that the Cr, Mo, and Si elements at 1200°C were higher than at 1080°C or 1200°C. This meant that the elemental diffusion of the Cr, Mo, and Si had an increasing effect on the precipitation of the σ phase at 1200°C at a cooling rate of $0.1^{\circ}C\,s^{-1}$, as represented in Table 2 [51].

2.10.2. Effect of Tensile Strain Rate and Time on the σ Phase. Hong and Han [52] conducted a high-temperature tensile test in superduplex stainless steel (Fe-24Cr-7Ni-3Mo-0.14N) at 850°C with a strain rate of $3.16\times10^{-3}\,s^{-1}$. The grain size of the σ phase increased in a deformed sample and maintained a constant value in the undeformed sample. This was because the controlled grain boundaries slip-strain induced the grain growth [53, 54] during the super-plasticity. Chandra and Kuchlmayr [55] reported that the σ phase content decreased with an increase in strain rate when the aging temperature was 900°C in Fe-19Cr-5Ni-2.7Mo stainless steel.

2.10.3. Effect of Cold Rolling Ratios on the σ Phase. Abe et al. [56] reported on the effect of various cold rolling ratios on the precipitation of the σ phase in Fe-10Cr-30Mn stainless steel. Experimental result indicated the LAXRD (Low-angle X-Ray Diffraction) analysis at 923 K under various cold rolling ratios and aging times (30% CW-10 h, 30% CW-100 h, 30% CW-1000 h, and 80% CW-1000 h). The CW is an abbreviation of the "Cold Working." The diffraction angle (2θ) of the LAXRD analysis is smaller than 85°, and this analytical method can show a clear diffraction signal. Many σ diffracted peaks can be detected, and there is no diffracted peak in the second phases. The diffracted peak of the σ phase is more obvious with 30% CW with an increase in aging time, which means that the precipitation of the σ phase does not decrease. Hence, cold rolling promotes the precipitation of the σ phase. Other diffracted peaks ($\sigma(410)$, $\sigma(212)$) of the σ phase were examined when the cold rolling ratio increased to 80% CW, and the $\sigma(312)$ peak was higher.

Figure 13 shows the TEM image in Fe-10Cr-30Mn stainless steel heat treated at 923 K for 3600 ks after cold rolling with various cold rolling ratios. The result shows that the grain size of the σ phase becomes smaller with increases in the cold rolling ratio, but that the distribution density of the σ phase increases. However, recrystallization only occurs above 30% CW, and there is no recrystallization with 10% CW. The σ phase only precipitates at the grain boundaries and triple points, as shown in Figure 13(a). A complete recrystallization happens with 60% CW and 80% CW, and then partial recrystallization occurs with 30% CW, as indicated in Figures 13(b)–13(d).

Huang and Chen [57] pointed out that cold working promoted the formation of the σ phase because the recrystallized and cold working boundaries were nucleated sites for the σ phase at low temperatures. At high temperatures, fine recrystallized grains formed and increased the area of the grain boundary so that the σ phase nucleated easily. Duhaj et al. [7] reported that the formation of the σ phase accelerated when the cold working degree was increased and that the σ phase content increased at the same time. It was concluded that the defects of stacking fault and twin acted as nucleation sites of the σ phase.

Figures 14(a)–14(c) show the relationship between recrystallization and the σ phase precipitation [56]. Initially, the σ phase nucleates at the recrystallized boundaries when crystallization occurs during cold rolling, as shown in Figure 14(a). This precipitation of the σ phase occurs because of the minimum strain energy during cold rolling. When the σ phase is formed, the recrystallized boundaries move to the deformed grains as a function of the recrystallized driving force (f_R). A recrystallized reacting force ($-f_p$) is also applied to the front of the recrystallized boundaries, as indicated in Figure 14(b). This recrystallized reacting force is due to the difference of the dislocation density from two sides of the recrystallized boundaries. Finally, the σ phase finishes the nucleation and grain growth and then escapes the recrystallized boundaries, as shown in Figure 14(c).

Koutsoukis et al. [58] studied the precipitation of the σ phase in S32654 super austenite stainless steel, cold rolled and aged at 850°C during cold rolling. The experimental result showed that the dispersion of the σ phase was more obvious when the cold rolling ratios were increased from 20% CW to 60% CW. The precipitation of the σ phase

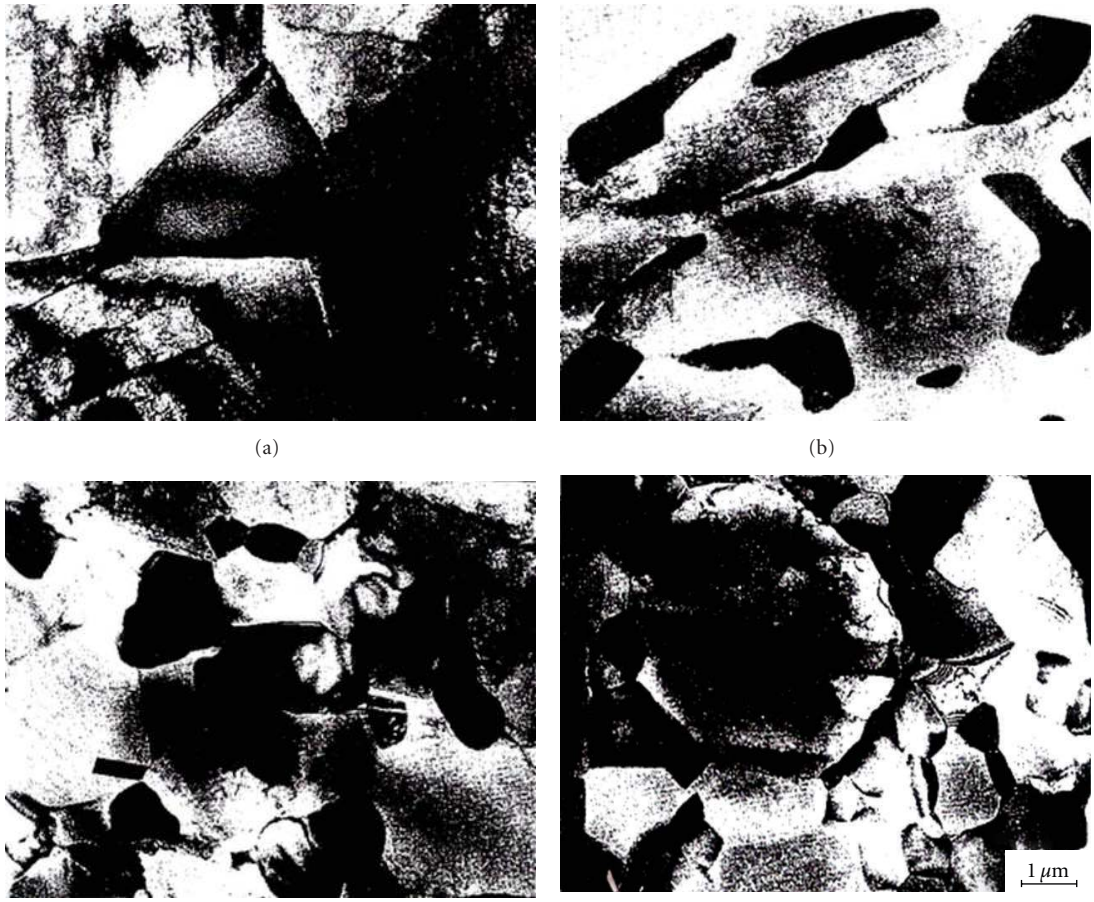

Figure 13: The effect of various cold rolling ratios on distribution and grain size of the σ phase (a) 10% CW, (b) 30% CW, (c) 60% CW, and (d) 80% CW [56].

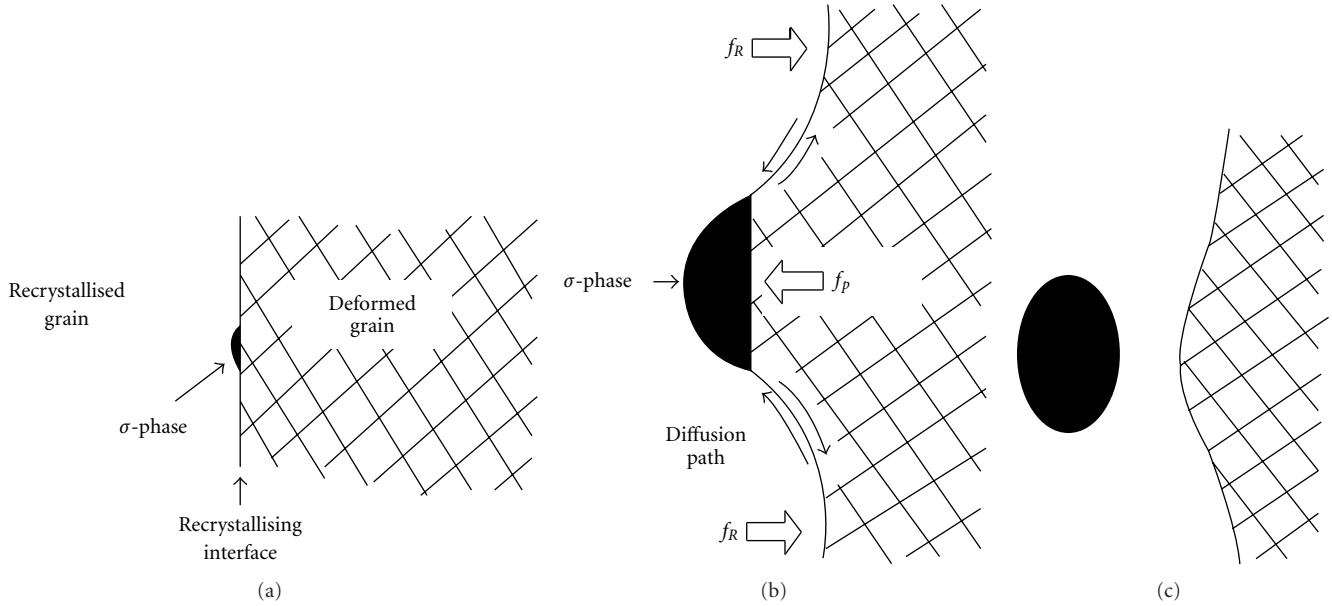

Figure 14: Nucleation and grain growth of σ phase at the recrystallized boundaries (f_R: recrystallized driving force, $-f_p$: recrystallized reacting force) [56].

increased the hardness value about 500 HV with 60% CW when aged at 650°C.

2.10.4. Effect of Hot Rolling Ratios on the σ Phase. Hsieh et al. [59] studied the precipitation mechanism of the σ phase in 19Cr-9Ni-2Mn austenitic and 18Cr-0.75Si ferritic stainless steels, hot rolled at 800°C under hot rolling ratios of 0%, 50%, and 75%. The experimental results indicated that the precipitation tendencies of the σ phase increased gradually with increase of the hot rolling ratio.

Experimental results show the morphological variations of the σ phase with hot rolling ratios of 0%, 50%, and 75% in 19Cr-9Ni-2Mn stainless steel. The morphologies of the σ phase changed from complete dendrites into fine globular structures when the hot rolling ratio was increased from 0% to 75%, with similar results in 18Cr-0.7Si stainless steel.

Hsieh et al. [60] pointed out that the dendrite σ phase was an unstable morphology and that the globular σ phase was a stable morphology. Gill et al. [61] also reported that the globular σ phase resulted from a refinement of the unstable σ phase. The globular σ phase consumed the Cr content of the δ-ferrite completely. Hence, the globular σ phase was maintained in the rolled state samples. Furthermore, the dendrite σ phase occurred because of the partial consumption of the Cr content of the δ-ferrite.

3. Summary

The above review has presented a clear overview of the precipitation of the σ phase in stainless steels. This review paper has provided the metallographic characteristics, precipitation mechanisms, properties effects, and prediction methods of the σ phase in stainless steels. The precipitation of the σ phase is the main reason for the degradation of stainless steels. Understanding the precipitation of the σ phase will allow for some control over the properties of stainless steels.

Acknowledgments

The authors would like to thank the National Science Council of the Taiwan, R.O.C. for financial support under Projects numbered NSC 100-ET-E-005-001-ET, NSC 101-2623-E-005-002-ET, NSC 100-2811-E-005-001, and NSC 101-2811-E-005-001. They are also obligated to thank Prof. Weite Wu and Prof. Dong-Yih Lin for their scientific writing guidance about this review paper.

References

[1] W. Treitschke and G. Tammann, "Enthalpy of formation for σ-phase solid solutions at 1060 K," *Anorganische Chemie*, vol. 55, p. 707, 1907.

[2] E. C. Bain and W. E. Griffiths, "An introduction to the Iron-Chromium Nickel alloys," *Transactions American Institute of Mining, Metallurgical and Petroleum Engineers*, vol. 75, pp. 166–213, 1927.

[3] E. R. Jett and F. Foote, "The Fe-Cr alloy system," *Metals and Alloys*, vol. 7, pp. 207–210, 1936.

[4] K. Yano and K. Abiko, "Role of carbon and nitrogen on the transformation of the σ phase in highly purified Fe-50 mass% Cr alloys," *Materials Transactions*, vol. 41, no. 1, pp. 122–129, 2000.

[5] B. Hattersley and W. Hume-Rothery, "Constitution of certain austenitic steels," *The Journal of the Iron and Steel Institute*, vol. 204, pp. 683–701, 1966.

[6] E. O. Hall and S. H. Algie, "The sigma phase," *International Materials Reviews*, vol. 11, pp. 61–88, 1966.

[7] P. Duhaj, J. Ivan, and E. Makovicky, "Sigma phase precipitation in austenitic steels," *The Journal of the Iron and Steel Institute*, vol. 206, pp. 1245–1252, 1968.

[8] M. E. Wilms, V. J. Gadgil, J. M. Krougman, and F. P. Ijsseling, "The effect of σ-phase precipitation at 800°C on the corrosion resistance in sea-water of a high alloyed duplex stainless steel," *Corrosion Science*, vol. 36, no. 5, pp. 871–881, 1994.

[9] C. M. Souza, H. F. G. Abreu, S. S. M. Tavares, and J. M. A. Rebello, "The σ phase formation in annealed UNS S31803 duplex stainless steel: texture aspects," *Materials Characterization*, vol. 59, no. 9, pp. 1301–1306, 2008.

[10] J. Lee, I. Kim, and A. Kimura, "Application of small punch test to evaluate sigma-phase embrittlement of pressure vessel cladding material," *Journal of Nuclear Science and Technology*, vol. 40, no. 9, pp. 664–671, 2003.

[11] D. Peckner and I. M. Bernstein, *Handbook of Stainless Steels*, McGraw-Hill, New York, NY, USA, 1st edition, 1977.

[12] M. H. Lewis, "Precipitation of (Fe, Cr) sigma phase from austenite," *Acta Metallurgica*, vol. 14, no. 11, pp. 1421–1428, 1966.

[13] F. B. Waanders, S. W. Vorster, and H. Pollak, "The influence of temperature on σ-phase formation and the resulting hardening of Fe-Cr-Mo-alloys," *Hyperfine Interactions*, vol. 120-121, no. 1–8, pp. 751–755, 1999.

[14] K. Shinohara, T. Seo, and K. Kumada, "Recrystallization and sigma phase formation as concurrent and interacting phenomena in 25%Cr-20%Ni steel," *Materials Transactions*, vol. 20, no. 12, pp. 713–723, 1979.

[15] E. Baerlecken and H. Fabritius, "Umwandlungskinetik der sigmaphase in einer Eisen-Chrom-Legierung mit 48% Chrom," *Arch Eisenhüttenwes*, vol. 26, pp. 679–686, 1955.

[16] C. M. Garzón and A. J. Ramirez, "Growth kinetics of secondary austenite in the welding microstructure of a UNS S32304 duplex stainless steel," *Acta Materialia*, vol. 54, no. 12, pp. 3321–3331, 2006.

[17] E. Folkhard, *Welding Metallurgy of Stainless Steels*, Springer, New York, NY, USA, 1st edition, 1988.

[18] J. Barcik, "Mechanism of σ-phase precipitation in Cr-Ni austenitic steels," *Materials Science and Technology*, vol. 4, no. 1, pp. 5–15, 1988.

[19] V. K. Sikka, M. G. Cowgill, and B. W. Roberts, "Creep properties of modified 9Cr-1Mo Steel," in *Proceedings of Topical Conference on Ferritic alloys for Use in Nuclear Energy Technologies*, ASM International, 1983.

[20] Y. S. Sato, H. Kokawa, K. Okamoto, S. Hirano, and M. Inagaki, "Rapid formation of the sigma phase in 304 stainless steel during friction stir welding," *Scripta Materialia*, vol. 49, no. 12, pp. 1175–1180, 1999.

[21] Y. S. Na, N. K. Park, and R. C. Reed, "Sigma morphology and precipitation mechanism in Udimet 720Li," *Scripta Materialia*, vol. 43, no. 7, pp. 585–590, 2000.

[22] A. F. Padilha and P. R. Rios, "Decomposition of austenite in austenitic stainless steels," *ISIJ International*, vol. 42, no. 4, pp. 325–337, 2002.

[23] B. Weiss and R. Stickler, "Phase instabilities during high temperature exposure of 316 austenitic stainless steel," *Acta Metallurgica*, vol. 3, no. 4, pp. 851–866, 1972.

[24] R. J. Gray, V. K. Sikka, and R. T. King, "Detecting transformation of delta-ferrite to sigma phase in stainless steels by advanced metallographic techniques," *Journal of Metals*, vol. 30, no. 11, pp. 18–26, 1978.

[25] C. C. Hsieh, *The study of δ/σ/γ phase transformation in 309LSi stainless steels after aging under nitrogen atmospheres*, M.S. thesis, I-Shou University, Taiwan, 2004.

[26] X. Tang, "Sigma phase characterization in AISI 316 stainless steel," *Microscopy and Microanalysis*, vol. 11, no. 2, pp. 78–79, 2005.

[27] C. C. Hsieh, D. Y. Lin, and W. Wu, "Dispersion strengthening behavior of σ phase in 304 modified stainless steels during 1073 K hot rolling," *Metals and Materials International*, vol. 13, no. 5, pp. 359–363, 2007.

[28] C. J. Park, M. K. Ahn, and H. S. Kwon, "Influences of Mo substitution by W on the precipitation kinetics of secondary phases and the associated localized corrosion and embrittlement in 29% Cr ferritic stainless steels," *Materials Science and Engineering A*, vol. 418, no. 1-2, pp. 211–217, 2006.

[29] C. C. Hsieh, D. Y. Lin, and T. C. Chang, "Microstructural evolution during the $\delta/\sigma/\gamma$ phase transformation of the SUS 309LSi stainless steel after aging under various nitrogen atmospheric ratios," *Materials Science and Engineering A*, vol. 475, no. 1-2, pp. 128–135, 2008.

[30] Y. S. Sato and H. Kokawa, "Preferential precipitation site of sigma phase in duplex stainless steel weld metal," *Scripta Materialia*, vol. 40, no. 6, pp. 659–663, 1999.

[31] J. Barcik, "The kinetics of σ-phase precipitation in AISI 310 and AISI 316 steels," *Metallurgical Transactions*, vol. 14, no. 4, pp. 635–641, 1983.

[32] D. M. E. Villanueva, F. C. P. Junior, R. L. Plaut, and A. F. Padilha, "Comparative study on sigma phase precipitation of three types of stainless steels: austenitic, superferritic and duplex," *Materials Science and Technology*, vol. 22, no. 9, pp. 1098–1104, 2006.

[33] A. L. Shaeffler, "Constitution diagram for stainless steel weld metal," *Metal Progress*, vol. 56, pp. 680–681, 1949.

[34] S. Konosu, H. Mashiba, M. Takeshima, and T. Ohtsuka, "Effects of pretest aging on creep crack growth properties of type 308 austenitic stainless steel weld metals," *Engineering Failure Analysis*, vol. 8, no. 1, pp. 75–85, 2001.

[35] M. C. Mataya and Martin J. Carr, "Characterization of inhomogeneities in complex austenitic stainless steel forgings," in *Deformation, Processing, and Structure*, ASM Materials Science Seminar, St. Louis, Mo, USA, 1982.

[36] G. S. Reis, A. M. Jorge, and O. Balancin, "Influence of the microstructure of duplex stainless steels on their failure characteristics during hot deformation," *Materials Research*, vol. 3, pp. 31–35, 2000.

[37] N. Lopez, M. Cid, and M. Puiggali, "Influence of σ-phase on mechanical properties and corrosion resistance of duplex stainless steels," *Corrosion Science*, vol. 41, no. 8, pp. 1615–1631, 1999.

[38] K. Ravindranath and S. N. Malhotra, "Influence of aging on intergranular corrosion of a 25% chromium-5% nickel duplex stainless steel," *Corrosion*, vol. 50, no. 4, pp. 318–328, 1994.

[39] J. T. Gow and O. E. Harder, "Balancing the composition of cast 25 per cent chromium-12 per cent nickel type alloys," *Transactions of the American Society for Metals*, vol. 30, pp. 855–935, 1942.

[40] L. R. Woodyatt, *Austenitic Stainless Steels: Microstructure and Mechanical Properties*, Springer, London, UK, 1st edition, 1984.

[41] F. C. Hull, "The effect of δ-ferrite on the hot cracking of stainless steel," *Welding Journal*, vol. 46, pp. 399s–409s, 1980.

[42] R. Badji, M. Bouabdallah, B. Bacroix, C. Kahloun, K. Bettahar, and N. Kherrouba, "Effect of solution treatment temperature on the precipitation kinetic of σ-phase in 2205 duplex stainless steel welds," *Materials Science and Engineering A*, vol. 496, no. 1-2, pp. 447–454, 2008.

[43] T. P. S. Gill, M. Vijayalakshmi, J. B. Gnanamoorthy, and K. A. Padmanabhan, "Transformation of delta-ferrite during the postweld heat treatment of type 316L stainless steel weld metal," *Welding Journal*, vol. 65, no. 5, pp. 122–128, 1986.

[44] D. Y. Lin, G. L. Liu, T. C. Chang, and H. C. Hsieh, "Microstructure development in 24Cr-14Ni-2Mn stainless steel after aging under various nitrogen/air ratios," *Journal of Alloys and Compounds*, vol. 377, no. 1-2, pp. 150–154, 2004.

[45] H. Brandis, W. Heimann, and E. Schmidtmann, "Effect of nitrogen on the precipitation behavior of steel X3CrNiMoNbN23 17," *TEW-Technische Berichte*, vol. 2, no. 2, pp. 150–166, 1976.

[46] O. Smuk, P. Nenonen, H. Hänninen, and J. Liimatainen, "Microstructures of a powder metallurgy-hot-isostatically pressed super duplex stainless steel forming in industrial heat treatments," *Metallurgical and Materials Transactions A*, vol. 35, no. 7, pp. 2103–2109, 2004.

[47] SGTE Solution Database, Department of Materials Science and Engineering, Royal Institute of Technology, Stockholm, Sweden.

[48] M. Lindholm, "A description of the thermodynamics of some Si containing systems," Licentiate thesis, Royal Institute of Technology, Stockholm, Sweden, 1995.

[49] J. Erneman, M. Schwind, L. Nylöf, J.-O. Nilsson, H.-O. Andrén, and J. Ågren, "Comparison between quantitative metallography and modeling of σ-phase particle growth in AISI 347 stainless steel," *Metallurgical and Materials Transactions A*, vol. 36, no. 10, pp. 2595–2600, 2005.

[50] N. Saunders and A. P. Miodownik, *CALPHAD (Calculation of Phase Diagrams) A Comprehensive Guide*, Elsevier Science, 1st edition, 1998.

[51] T. H. Chen and J. R. Yang, "Effects of solution treatment and continuous cooling on σ-phase precipitation in a 2205 duplex stainless steel," *Materials Science and Engineering A*, vol. 311, no. 1-2, pp. 28–41, 2001.

[52] S. H. Hong and Y. S. Han, "Phenomena and mechanism on superplasticity of duplex stainless steels," *Metals and Materials International*, vol. 6, no. 2, pp. 161–167, 2000.

[53] K. Holm, J. D. Embury, and G. R. Purdy, "The structure and properties of microduplex Zr-Nb alloys," *Acta Metallurgica*, vol. 25, no. 10, pp. 1191–1200, 1977.

[54] J. R. Spingarn and W. D. Nix, "Diffusional creep and diffusionally accommodated grain rearrangement," *Acta Metallurgica*, vol. 26, no. 9, pp. 1389–1398, 1978.

[55] T. Chandra and R. Kuchlmayr, "Effect of strain rate on sigma formation in ferrite-austenite stainless steel at high temperatures," *Journal of Materials Science*, vol. 23, no. 2, pp. 723–728, 1988.

[56] F. Abe, H. Arki, and T. Noda, "Discontinuous precipitation of σ-phase during recrystallization in cold rolled Fe-10Cr-30 Mn austenite," *Materials Sciences and Technology*, vol. 4, pp. 885–893, 1988.

[57] C. S. Huang and H. C. Chen, "A discussion on stainless steels welding (II)," *Welding and Cutting*, vol. 8, pp. 48–54, 1998.

[58] T. Koutsoukis, E. Papadopoulou, P. Kokkonidis, and G. Fourlaris, "Effect of ageing in cold rolled superaustenitic stainless steels," in *EMC 2008 14th European Microscopy Congress*, S. Zormalia, Ed., pp. 451–452, Springer, Berlin, Germany, 2008.

[59] C. C. Hsieh, D. Y. Lin, and W. Wu, "Precipitation behavior of σ phase in 19Cr-9Ni-2Mn and 18Cr-0.75Si stainless steels hot-rolled at 800°C with various reduction ratios," *Materials Science and Engineering A*, vol. 467, no. 1-2, pp. 181–189, 2007.

[60] C.C. Hsieh, D.Y. Lin, and W. Wu, "Precipitation behavior of sigma phase in 304 and 430 stainless steels as hot-rolled at 800°C," in *Proceedings of the American Physical Society (APS '07)*, Colorado Convention Center, March 2007.

[61] T. P. S. Gill, M. Vijayalkshmi, P. Rodriguez, and K. A. Padmanabhan, "On microstructure-property correlation of thermally aged type 316L stainless steel weld metal," *Metallurgical Transactions A*, vol. 20, no. 6, pp. 1115–1124, 1989.